RSC Advances

ROYAL SOCIETY OF CHEMISTRY

www.rsc.org/advances

Graphical abstract:

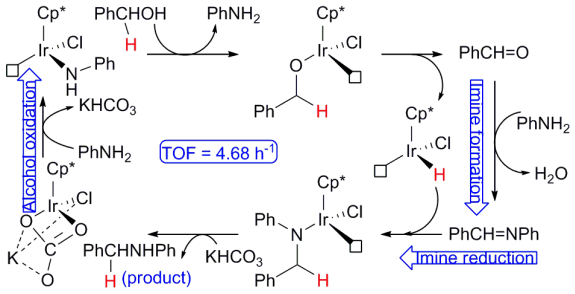

Using DFT methods and the energetic span model, the most favorable hydrogen autotransfer pathway for $[Cp^*IrCl_2]_2/K_2CO_3$-catalyzed N-alkylation of amines with alcohols has been found.

ARTICLE TYPE
www. rsc.org/xxxxxx | XXXXXXXX

Mechanistic study on Cp*iridium-catalyzed N-alkylation of amines with alcohols†

Guo-Ming Zhao,[a,b] Hui-ling Liu,*[a] Xu-ri Huang,[a] Dan-dan Zhang[a] and Xue Yang[b]

Received Xth XXXXXXXXXX 20XX, Accepted Xth XXXXXXXXX 20XX
First published on the web Xth XXXXXXXXXX 200X
DOI: 10.1039/b000000x

DFT calculations have been performed to study the mechanism of N-alkylation of amines with alcohols catalyzed by $[Cp^*IrCl_2]_2$ ($Cp^* = \eta^5$-C_5Me_5) in the present of K_2CO_3. The energetic results show that this N-alkylation reaction proceeds via the hydrogen autotransfer mechanism and the catalytic cycle includes three sequential stages: (1) alcohol oxidation to produce aldehyde, (2) aldehyde-amine condensation to form imine, (3) imine reduction to afford the secondary amine product. For stages 1 and 3, the most favorable pathways are the inner-sphere hydrogen transfer pathway under the catalysis of $Cp^*Ir(NHPh)Cl$ (**C**) and the inner-sphere hydrogen transfer pathway with $KHCO_3$ as the proton donor, respectively. Thermodynamically, both stages 1 and 2 are endergonic, but stage 3 is highly exergonic. Thus stage 3 is the driving force for the catalytic cycle. The energetic span model has also been used to assess the catalytic cycle, and it is found that the turnover frequency-determining intermediate (TDI) and the turnover frequency-determining transition state (TDTS) are the 18*e* complex $Cp^*Ir(\kappa^2$-$CO_3K)$ (**A**) and the transition state **BC-TS5i** for β-H elimination, respectively. The calculated turnover frequency (TOF), 4.68 h^{-1}, agrees with the experimentally determined TOF and, therefore, provides strong support for the proposed catalytic cycle.

1 Introduction

N-Alkylation of amines plays an important role in the syntheses of polymers, peptides, pharmaceuticals, pesticides, and functional materials.[1] N-Alkylated amines are usually prepared via the reaction of amines with alkyl halides[2] or the reductive amination with carbonyl compounds.[3] However, these two methods have some drawbacks: The former requires to use the toxic alkyl halides as the reactants and generates many inorganic salts as byproducts; The latter needs to use the expensive and unstable carbonyl compounds as the reactants and cannot always yield the monoalkylated products selectively. Alternatively, N-alkylated amines can also be synthesized through hydroaminations[4] or hydroaminomethylations.[5] In recent decades, much attention has been focused on N-alkylation of amines and their derivatives with alcohols based on a hydrogen autotransfer (also called borrowing hydrogen) mechanism.[6] This N-alkylated method is a very attractive candidate for the synthesis of amino derivatives because alcohols are nontoxic, inexpensive, and readily available and the only side product is theoretically water.

N-Alkylation of amines with alcohols was first reported by Grigg[7] and Watanabe[8] in 1981, respectively, and since then many homogeneous transition metal catalysts, such as palladium-,[9] ruthenium-,[10] rhodium-,[11] iridium-,[12–17] copper-,[18] or iron-based[19] complexes, have been used for such an environmentally friendly process. Among these catalysts, one of the most famous is the dimeric iridium complex $[Cp^*IrCl_2]_2$. Since it was found to have a catalytic activity toward hydrogen transfer reactions between organic molecules in 2002,[20] $[Cp^*IrCl_2]_2$ has been applied in N-alkylation of amines,[13,14] sulfonamides,[15] and ammonium salts[16] with alcohols as the alkylation reagents and the desired products are obtained in good yields. Some other Cp^*Ir complexes with functionalized ligands also exhibit high catalytic activity in the N-alkylation reactions of amines with alcohols.[17] Thus, Cp^*Ir complexes-catalyzed N-alkylation of amines with alcohols is of significant importance.

Detailed mechanistic studies will help to promote development of catalytic systems. In 2008, Eisenstein and coworkers performed a DFT mechanistic study on N-alkylation of amines with alcohols catalyzed by $[CpIrCl_2]_2/K_2CO_3$ (Cp = C_5H_5).[21] Their calculation results showed that the dissociation energies of CH_3OH from $CpIr(\kappa^2$-$CO_3)(CH_3OH)$ and CH_3NH_2 from $CpIr(\kappa^2$-$CO_3)(CH_3NH_2)$ were 8.0 and 23.4 kcal mol^{-1}, respectively. Then they believed that "the amine inhibited the reaction by disfavoring the coordination of the alcohol". Their calculation results also showed that the dissociation energy of the product $NHMe_2$ from

† Electronic Supplementary Information (ESI) available: Detailed optimized geometries, energies, thermal corrections to enthalpies and free energies, the energetic span model, and Fortran program for TOF and X_i calculations. See DOI: 10.1039/b000000x/

[a] *State Key Laboratory of Theoretical and Computational Chemistry, Institute of Theoretical Chemistry, Jilin University, Changchun, China. E-mail: huiling@jlu.edu.cn*
[b] *College of Science, Jilin Institute of Chemical Technology, Jilin, China.*

$CpIr(\kappa^2\text{-}CO_3)(NHMe_2)$, 22.1 kcal mol^{-1}, was lower than that of CH_3NH_2 from $CpIr(\kappa^2\text{-}CO_3)(CH_3NH_2)$. However, they still argued that "the dissociation of $NHMe_2$ from $CpIr(\kappa^2\text{-}CO_3)(NHMe_2)$ was the rate-determining step". In 2012, Madsen and coworkers also studied the mechanism of N-alkylation of amines with alcohols catalyzed by $[Cp^*IrCl_2]_2/K_2CO_3$ experimentally and computationally.[22] They believed that an amine as the ligand of the catalyst took part in the catalytic process, which was different from Eisenstein and coworkers' conclusion–the amine inhibited the reaction by disfavoring the coordination of an alcohol. However, their DFT study is incomplete because the proton transfer processes of alcohol oxidation and imine reduction are not calculated in their research. Therefore, a further mechanistic study on $[Cp^*IrCl_2]_2$-catalyzed N-alkylation of amines with alcohols is urgently needed.

Inspired by the mechanistic studies of Ir-,[21–23] Cu-,[24] and Ru-catalyzed[25] hydrogen transfer reactions, we carry out a thorough DFT mechanistic study on $[Cp^*IrCl_2]_2$-catalyzed N-alkylation of amines with alcohols. Our purposes are as follows: (1) to elucidate the roles of the base and the amine ligand, (2) to locate the active catalyst, (3) to seek the most favorable reaction pathway, (4) to identify the TDI and the TDTS, (5) to point out the driving force of the catalytic cycle.

2 Computational details

All calculations were carried out using Gaussian09 suite of programs.[26] Molecular geometries of all complexes were fully optimized with tight convergence criteria (scf=tight) at the B3LYP[27,28] /BSI (SMD,[29] toluene) level (BSI designates the basis set combination of SDD[30] for the Ir atom and 6-31G(d,p)[31] for the other atoms; SMD corresponds to Truhlar and coworkers' solvation model which does an IEFPCM calculation with radii and non-electrostatic terms). At the same level of theory, frequency calculations were performed to identify the stationary points to be real minima or transition states and to provide thermal corrections to enthalpies and Gibbs free energies at 383.15 K. When necessary, intrinsic reaction coordinate (IRC) calculations[32] were conducted to verify that a transition state connected its forward and backward minima on the free energy surface. Single-point energies of stationary points were calculated at the m06[33]/BSII(SMD,toluene) level (BSII designates the basis set combination of def2-QZVP[30,34] for the Ir atom and 6-311++G(2df,2p) for the other atoms). All energies used in this paper are the single-point energies corrected by Gibbs free energy corrections, unless otherwise specified. We also give the enthalpy results (single-point energies corrected by enthalpies corrections) in the figures for reference. To verify the functional and basis sets dependence, we carried out M06/BSIV//B3LYP/BSIII (BSIII: the basis set combination of SDDALL[30,35] with an extra f polarization basis function (exponent 0.938) for Ir and 6-31G(d,p) for all the other atoms; BSIV: the basis set combination of SDDALL with an extra f polarization basis function (exponent 0.938) for Ir and 6-311++G(2df,2p) for all the other atoms), M06/BSII//B3PW91[27,36]/BSI, M06/BSII//PBE1PBE[37]/BSI, and M06/BSII//M06/BSI calculations on selective species. The solvent model and the convergence criteria for those calculations were the same as above.

3 Results and discussion

3.1 Model reaction

Molecular geometries of reactants and a catalyst have a significant impact on the TOF of a catalytic cycle.[38] Thus the experimental reactants and catalyst were used in this calculations without any simplification. As shown in eq 1, $[Cp^*IrCl_2]_2$ and

$$PhNH_2 + PhCH_2OH \xrightarrow[\text{toluene,110°C,17h}]{\text{[Cp*IrCl}_2\text{]}_2\text{ (5.0 mol\%Ir)},\ K_2CO_3\text{ (5.0 mol\%)}} PhCH_2NHPh + H_2O \qquad (1)$$

K_2CO_3 were employed as the catalyst precursor and the base, respectively, and N-alkylation of $PhNH_2$ with $PhCH_2OH$ was chosen as the model reaction.

3.2 Alcohol oxidation

3.2.1 Catalyst initiation. In the DFT study on Ir-catalyzed N-alkylation reaction of amines with alcohols, Eisenstein and co-workers postulated three possible Ir cata-

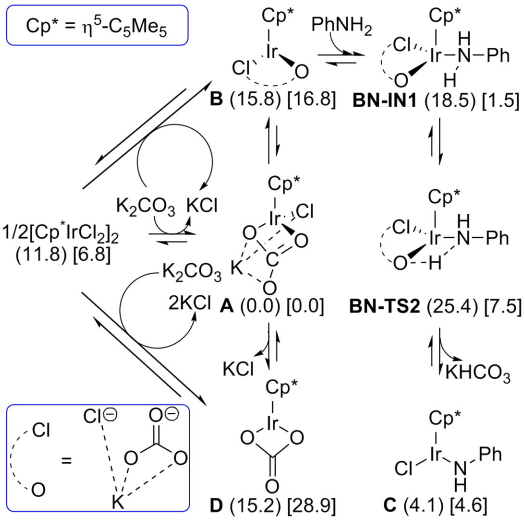

Fig. 1 Catalyst initiation. Values in parentheses and square brackets are Gibbs free energies and enthalpies in kcal mol^{-1}, respectively.

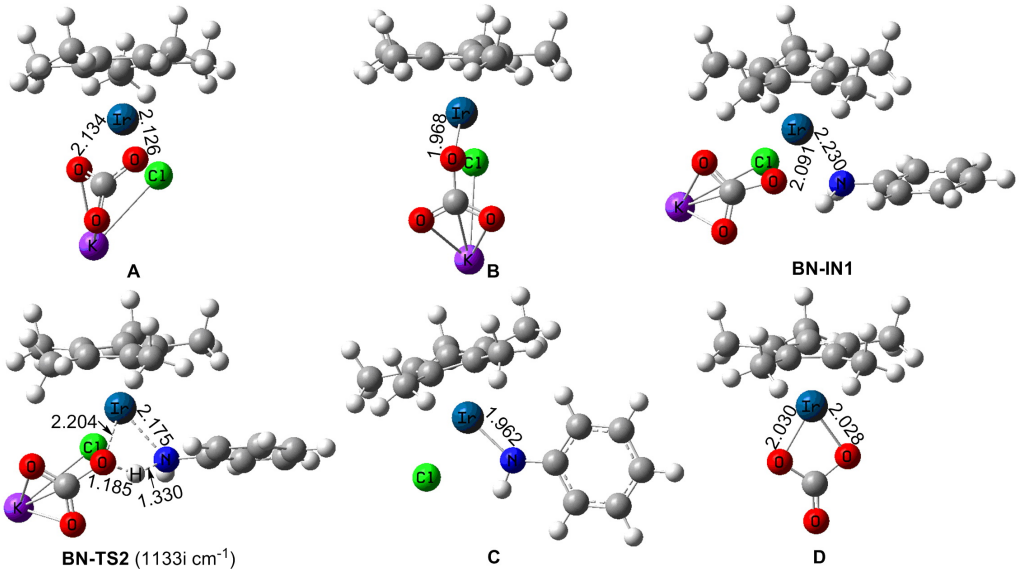

Fig. 2 Optimized geometries of Cp*Ir complexes with selected bond distances (in Å).

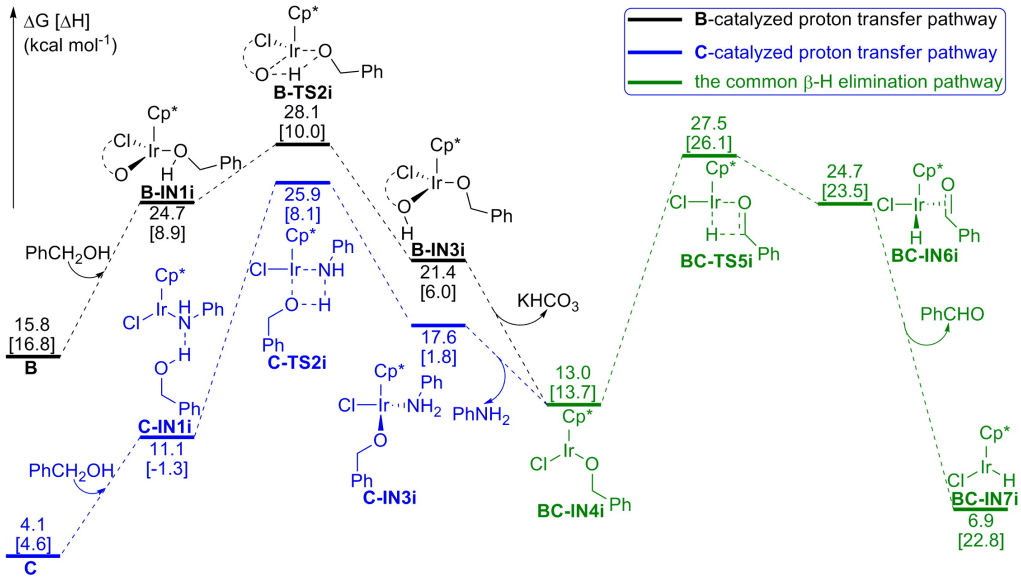

Fig. 3 Free energy profiles for **B**- and **C**-catalyzed benzyl alcohol oxidation via the inner-sphere hydrogen transfer pathways.

lysts: CpIr(κ^2-CO_3), $CpIrCl_2$, and CpIr(NH_2Me)$(Cl)^+$, and found that CpIr(κ^2-CO_3) was the active catalyst.[21] To contrast with Eisenstein and co-workers' work, Cp*Ir(κ^2-CO_3) (**D**) was postulated as the possible catalyst in this study. Meanwhile, we also proposed two other possible catalysts: Cp*Ir(κ^1-CO_3K) (**B**) and **C**. The correlations between **B**, **C**, and **D** are shown in Fig. 1. The dimer 1/2$[Cp^*IrCl_2]_2$ can switch to the monomer **A** in the presence of K_2CO_3, giving off a free energy of 11.8 kcal mol^{-1}. **A** is an 18*e* Ir chloride with a κ^2-CO_3K ligand, in which the lengths of the two Ir−O bonds are 2.126 and 2.134 Å, respectively (Fig. 2). The decoordination of the arm oxygen of the κ^2-CO_3K ligand can afford the κ^1-CO_3K-coordinated 16*e* Ir chloride **B** by costing a free energy of 15.8 kcal mol^{-1}. The 16*e* complex **C** can be obtained after passing through the $PhNH_2$-coordinated intermediate **BN-IN1** and the transition state **BN-TS2** for proton transfer. The Ir−N bonds in **BN-IN1**, **BN-TS2**, and **C** are 2.230, 2.175, and 1.962 Å, respectively, and the Ir−O bonds

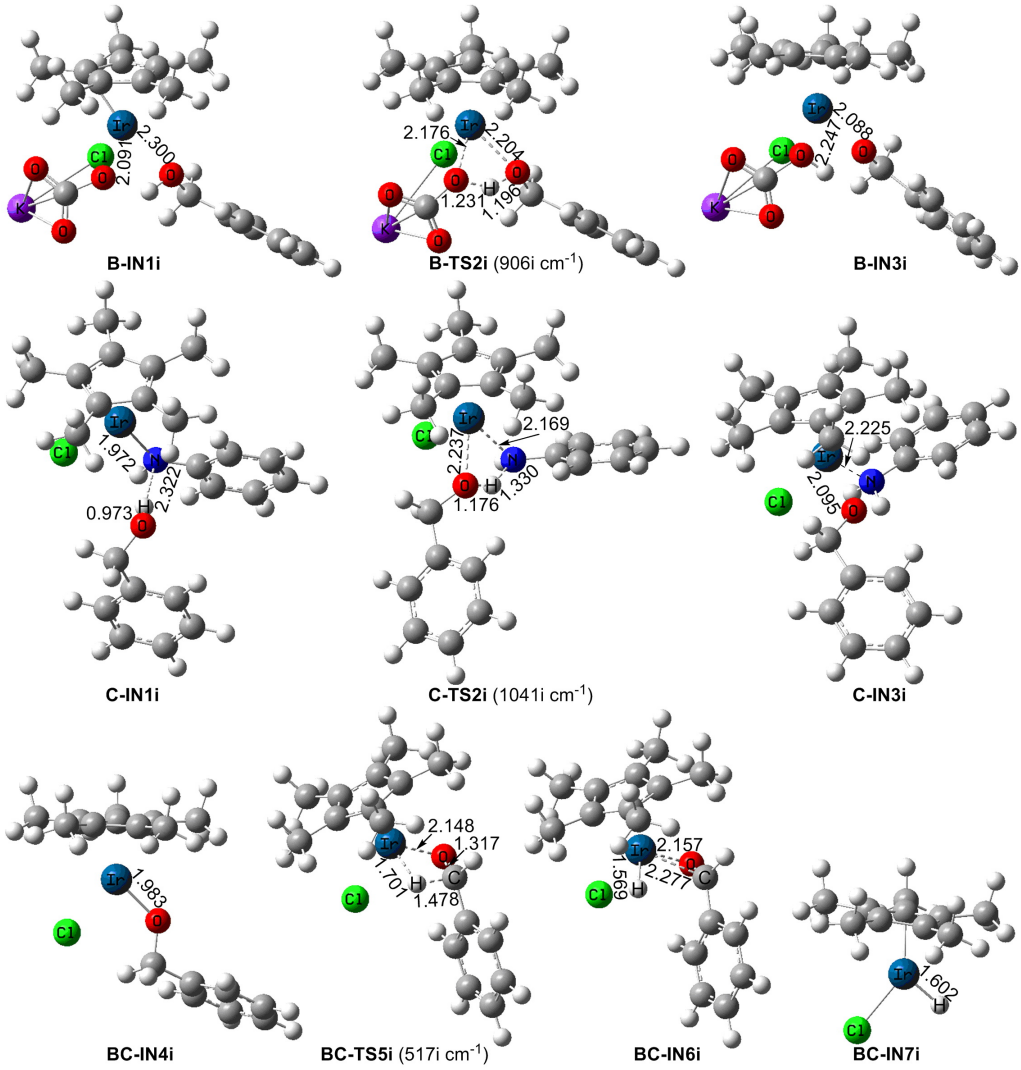

Fig. 4 Optimized structures of the stationary points with selected bond distances (in Å) for **B**- and **C**-catalyzed benzyl alcohol oxidation via the inner-sphere hydrogen transfer pathways.

in **B**, **BN-IN1**, and **BN-TS2** are 1.968, 2.091, and 2.204 Å, respectively, indicating that the formation of the Ir−N bond accompanies the dissociation of the Ir−O bond. The free energies of **BN-IN1** and **BN-TS2**, relative to **A** + $PhNH_2$, are 18.5 and 25.4 kcal mol^{-1}, respectively, which shows that the formation of **C** is feasible in kinetics under the experimental conditions (see eq 1). Overall, the formation of **C** (**A** + $PhNH_2 \rightarrow$ **C** + $KHCO_3$) is endergonic by only 4.1 kcal mol^{-1}. The 16*e* Ir complex **D** can be formed by dissociating a molecule of KCl from **A** with a free energy change of 15.2 kcal mol^{-1}. Note that **A** has the lowest free energy among all the Ir complexes, so it is chosen as the energy reference point in the above and following discussions.

3.2.2 Inner-sphere alcohol oxidation. With the postulated catalysts in hand, we now study the possible inner-sphere hydrogen transfer pathways for alcohol oxidation. The free energy profiles for **B**- and **C**-catalyzed benzyl alcohol oxidation via the inner-sphere hydrogen transfer pathways are shown in Fig. 3, and the corresponding optimized structures of the stationary points are displayed in Fig. 4. First, we consider the **B**-catalyzed proton transfer pathway, in which coordination of $PhCH_2OH$ to complex **B** gives the intermediate **B-IN1i** by costing a free energy of 8.9 kcal mol^{-1}. This complex is well prepared for the proton transfer. After passing through the transition state **B-TS2i** with a relative free energy of 3.4 kcal mol^{-1} to **B-IN1i**, the O−H bond of $PhCH_2OH$ breaks and the proton transfers to the O atom of the CO_3K ligand,

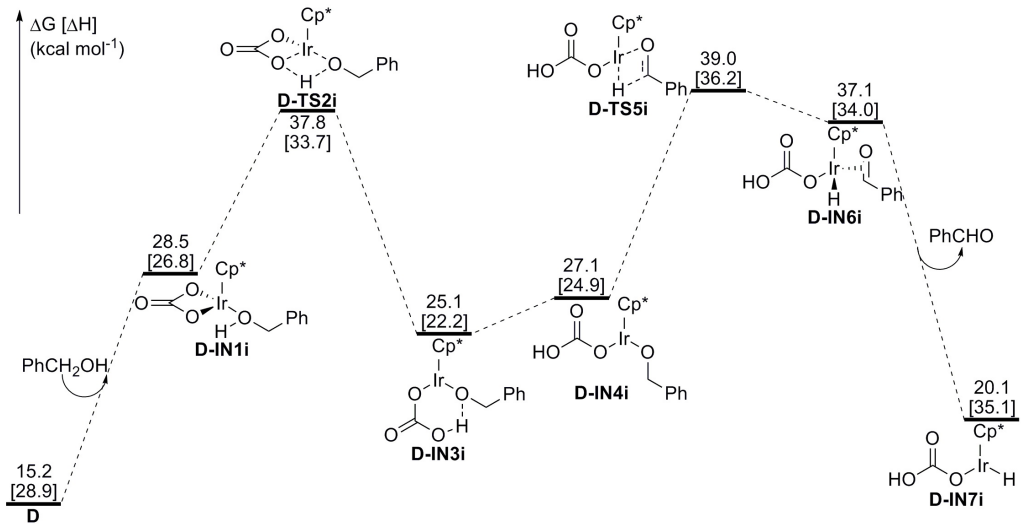

Fig. 5 Free energy profile for **D**-catalyzed benzyl alcohol oxidation via the inner-sphere hydrogen transfer pathway.

leading to the formation of the $KHCO_3$-coordinated complex **B-IN3i**, which can afford a more stable alkoxide intermediate **BC-IN4i** by releasing a molecule of $KHCO_3$.

The second scenario considered is the **C**-catalyzed proton transfer pathway. The binding of $PhCH_2OH$ to **C** with an OH···N hydrogen bond of 2.322 Å generates the initial complex **C-IN1i**. This binding process is favorable by 5.9 kcal mol^{-1} in enthalpy, but unfavorable by 7.0 kcal mol^{-1} in Gibbs free energy because of entropic effect. The transition state **C-TS2i** for the proton transfer is located at a free energy of 14.8 kcal mol^{-1} above **C-IN1i**, in which the proton lies midway between the anionic O and N ligands (O···H = 1.176 Å and N···H = 1.330 Å). This transition state leads to the formation of the $PhNH_2$-coordinated intermediate **C-IN3i**. The length of the Ir−O bond in **C-IN3i**, 2.095 Å, becomes much shorter than that in **C-TS2i**, 2.237 Å, while the distance of the Ir−N bond in **C-IN3i**, 2.225 Å, becomes longer than that in **C-IN1i**, 1.972 Å, and in **C-TS2i**, 2.169 Å. Although **C-IN3i** is 8.3 kcal mol^{-1} more stable than the transition state **C-TS2i**, the favorable entropy can provide the driving force for the $PhNH_2$ dissociation from **C-IN3i** to give the key alkoxide intermediate **BC-IN4i**. This dissociation lowers the system down by 4.6 kcal mol^{-1}.

Now, we consider the common β-H elimination pathway for **B**- and **C**-catalyzed alcohol oxidation. The transition state **BC-TS5i** for β-H elimination is located at a free energy of 14.5 kcal mol^{-1} above **BC-IN4i**, in which the C···H, Ir···H, and C−O distances are 1.478, 1.701, and 1.317 Å, respectively, confirming the C−H bond-breaking process and the Ir−H and C=O bond-forming processes. This transition state results in the PhCHO-coordinated Ir hydride **BC-IN6i**. The Ir−O and Ir−C distances in **BC-IN6i** are 2.157 and 2.277 Å, respectively, indicating the C=O bond coordinates to the Ir center. However, intermediate **BC-IN6i** is unstable, whose dissociation leads to the formation of the alcohol oxidation product PhCHO and the 16*e* Ir hydride intermediate **BC-IN7i**. This dissociation lowers the system down by 17.8 kcal mol^{-1}.

$CpIr(\kappa^2\text{-}CO_3)$-catalyzed alcohol oxidation has been studied by Eisenstein and co-workers with CH_3OH and CH_3NH_2 as the reagents.[21] Here, we reconsider the possibility of CO_3^{2-} as the ligand participating in alcohol oxidation using the experimental reagents and ligand (Cp^*). As shown in Fig. 5, the alcohol oxidation takes place stepwise by passing the

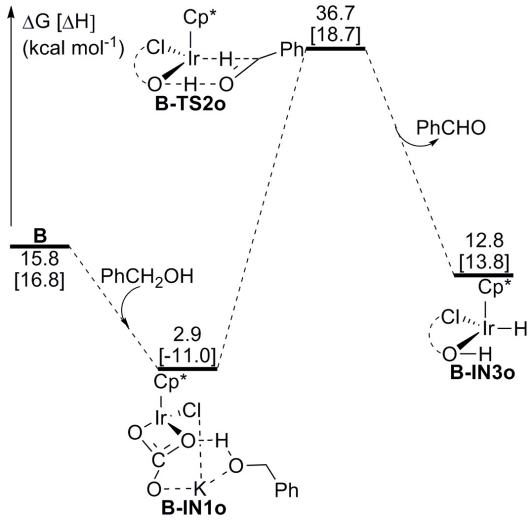

Fig. 6 Free energy profile for **B**-catalyzed benzyl alcohol oxidation via the outer-sphere hydrogen transfer pathway.

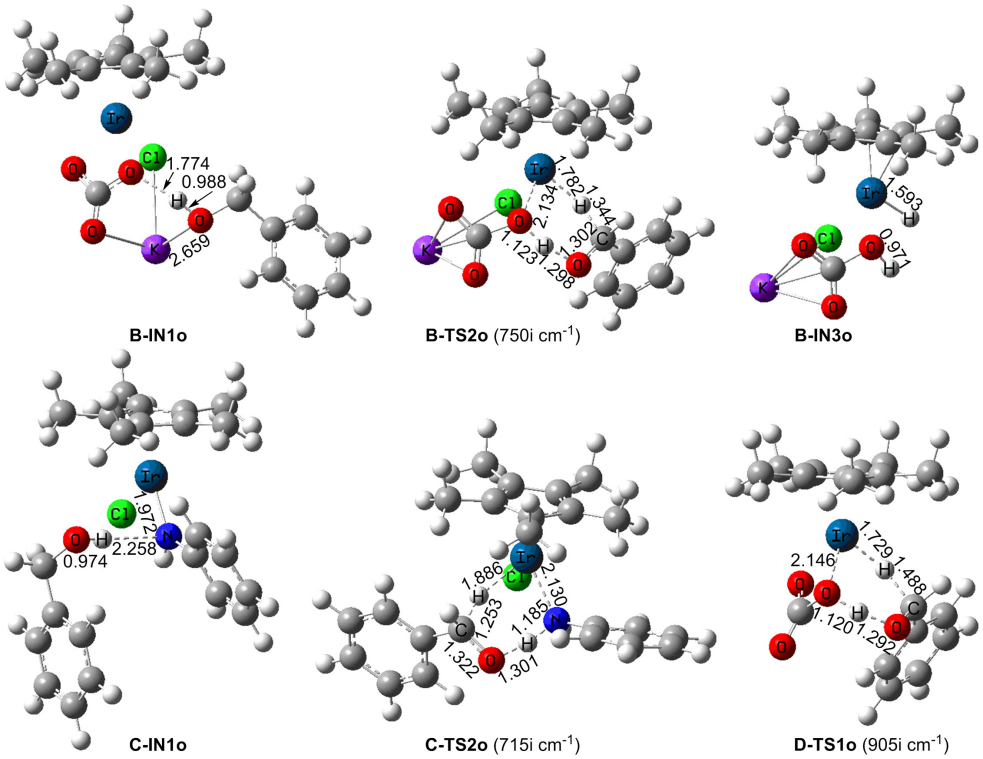

Fig. 7 Optimized structures of the key stationary points with selected bond distances (in Å) for the outer-sphere benzyl alcohol oxidation.

$PhCH_2OH$-coordinated intermediate **D-IN1i**, the transition state **D-TS2i** for proton transfer, the alkoxide intermediate **D-IN3i**, the alkoxide intermediate **D-IN4i**, the transition state **D-TS5i** for β-H elimination, and the PhCHO-coordinated Ir hydride **D-IN6i**. Relative to the energy reference point, the free energies of **D-IN1i**, **D-TS2i**, **D-IN3i**, **D-IN4i**, **D-TS5i**, and **D-IN6i** are 28.5, 37.8, 25.1, 27.1, 39.0, and 37.1 kcal mol^{-1}, respectively. This alcohol oxidation results in the formation of the alcohol oxidation product PhCHO and the Ir hydride species **D-IN7i** containing a κ^1-bicarbonate ligand.

3.2.3 Outer-sphere alcohol oxidation. In this section, we will consider the possible outer-sphere hydrogen transfer pathways for alcohol oxidation under the catalysis of **B**, **C**, and **D**, respectively. The first scenario considered is the **B**-catalyzed alcohol oxidation pathway. As shown in Fig. 6 and 7, the binding of $PhCH_2OH$ to **B** with a $(PhCH_2)O-K$ bond of 2.659 Å and an OH···O hydrogen bond of 1.774 Å gives the initial intermediate **B-IN1o**, which is 12.9 kcal mol^{-1} more stable than **B** + $PhCH_2OH$. The transition state **B-TS2o** for the concerted proton and hydride transfer is located at a free energy of 33.8 kcal mol^{-1} above **B-IN1o**. In this six-membered transition state, The distances of $PhCH_2O\cdots H$, $KO_2CO\cdots H$, C···H, and Ir···H are 1.298, 1.123, 1.344, and 1.782 Å, respectively. This transition state yields the alcohol oxidation product PhCHO and the $KHCO_3$-coordinated Ir hydride species **B-IN3o**.

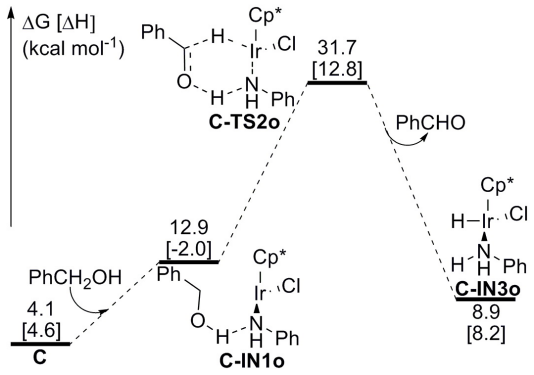

Fig. 8 Free energy profile for **C**-catalyzed benzyl alcohol oxidation via the outer-sphere hydrogen transfer pathway.

The second scenario considered is the **C**-catalyzed alcohol oxidation pathway. As shown in Fig. 7 and 8, $PhCH_2OH$ first binds to **C** with a OH···N hydrogen bond of 2.258 Å and simultaneously forms the initial intermediate **C-IN1o** by costing a free energy of 8.8 kcal mol^{-1}. The transition state **C-TS2o** for the concerted proton and hydride transfer has a six-

membered structure, in which the distances of O···H, N···H, C···H, and Ir···H are 1.301, 1.185, 1.253, and 1.886 Å, respectively, confirming the concerted proton and hydride transfer process. After passing through the transition state **C-TS2o** with a relative free energy of 18.8 kcal mol^{-1} to **C-IN1o**, the product of alcohol oxidation, PhCHO, and the $PhNH_2$-coordinated Ir hydride **C-IN3o** are generated.

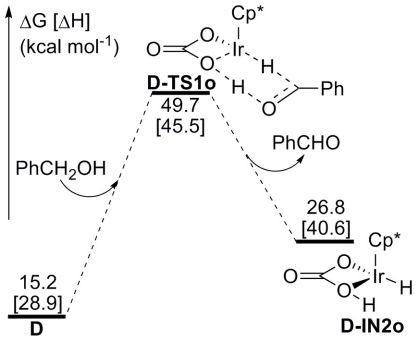

Fig. 9 Free energy profile for **D**-catalyzed benzyl alcohol oxidation via the outer-sphere hydrogen transfer pathway.

The final scenario considered is the **D**-catalyzed alcohol oxidation pathway. As displayed in Fig. 7 and 9, The transition state **D-TS1o** for the concerted proton and hydride transfer, located at a free energy of 34.5 kcal mol^{-1} above $PhCH_2OH$ + **D**, also has a six-membered structure, in which the distances of $PhCH_2O$···H, O_2CO···H, C···H, and Ir···H are 1.292, 1.120, 1.488, and 1.729 Å, respectively. This transition state delivers the alcohol oxidation product PhCHO and the Ir hydride **D-IN2o** containing a κ^2-bicarbonate ligand.

3.2.4 Comparison of different alcohol oxidation pathways. In the above discussions of alcohol oxidation, we postulated three possible catalysts (**B**, **C**, and **D**) and calculated the corresponding inner-sphere and outer-sphere hydrogen transfer pathways. The six complete pathways for alcohol oxidation are as follows: (1A) (Note: A denotes alcohol oxidation) the inner-sphere alcohol oxidation pathway under the catalysis of **B** (Fig. 1 (**A** → **B**) and 3 (black pathway + green pathway)), (2A) the inner-sphere alcohol oxidation pathway under the catalysis of **C** (Fig. 1 (**A** → **B** → **BN-IN1** → **BN-TS2** → **C**) and 3 (blue pathway + green pathway)), (3A) the inner-sphere alcohol oxidation pathway under the catalysis of **D** (Fig. 1 (**A** → **D**) and 5), (4A) the outer-sphere alcohol oxidation pathway under the catalysis of **B** (Fig. 1 (**A** → **B**) and 6), (5A) the outer-sphere alcohol oxidation pathway under the catalysis of **C** (Fig. 1 (**A** → **B** → **BN-IN1** → **BN-TS2** → **C**) and 8), and (6A) the outer-sphere alcohol oxidation pathway under the catalysis of **D** (Fig. 1 (**A** → **D**) and 9). For pathways 1A-6A, the activation free energy barriers are 28.1, 27.5, 39.0, 36.7, 31.7, and 49.7 kcal mol^{-1}, respectively, and the reaction free energies are 6.9, 6.9, 20.1, 12.8, 8.9, and 26.8 kcal mol^{-1}, respectively. On the basis of these calculation results, we can draw the following conclusions: (1) Although pathway 2A is endergonic, it is still the most favorable when compared with other alcohol oxidation pathways. The endergonic reason can be attributed to the formation of chemically more reactive aldehyde and Ir hydride species. (2) **C** is the active catalyst, in which one of the chloride ligands has been displaced by $PhNH^-$. The release of the chloride is in agreement with Fristrup and co-workers' experimental result.[22] (3) Pathway 1A is the second favorable alcohol oxidation pathway. (4) Other alcohol oxidation pathways cannot compete with 2A or 1A, thus becoming the unfavorable pathways.

Note that the difference between pathways 1A and 2A is that the CO_3K^- ligand is used as the proton acceptor in 1A, and the $PhNH^-$ ligand is used as the proton acceptor in 2A (Fig. 3). Thus, it is the $PhNH^-$ ligand lowering down the free energy barrier for the proton transfer that makes 2A is more favorable than 1A kinetically. The conclusion that a catalyst with a deprotonated reactant amine as the ligand may facilitate alcohol oxidation is consistent with our previous theoretical study.[24] If Cp*Ir active catalyst could be previously synthesized in toluene from $[Cp^*IrCl_2]_2$, K_2CO_3, and the corresponding reactant amine, Cp*Ir-catalyzed N-alkylation of amines with alcohols would be greatly accelerated. In fact, the reactant NH_3 was used as the ligand to synthesize the Cp*Ir catalyst in the multialkylation reaction of aqueous ammonia with alcohols as early as 2010.[39] Therefore, this study will provide useful information for the synthesis of novel catalysts.

3.3 Imine formation

The product of $PhCH_2OH$ oxidation, PhCHO, can readily react with $PhNH_2$ to give the imine PhCH=NPh and H_2O under the experimental conditions (see eq 1). And water-[40] and alcohol-catalyzed[41] condensation of aldehyde with amine to form imine and alcohol-mediated coupling of aldehyde with amine to generate amide[42] have been studied computationally. Therefore, we do not consider the condensation process (PhCHO + $PhNH_2$ → PhCH=NPh + H_2O) in detail here, but only calculate the reaction free energy–the overall imine formation process is endergonic by only 2.9 kcal mol^{-1}. In order to link the free energy profile for alcohol oxidation (pathway 2A) with a free energy profile for imine reduction, this energy has been directly added to the starting point of the free energy profile for imine reduction (see below).

3.4 Imine reduction

The above calculations show that the most favorable alcohol oxidation pathway is the inner-sphere hydrogen transfer pathway under the catalysis of **C**, so the Ir hydride **BC-IN7i** ob-

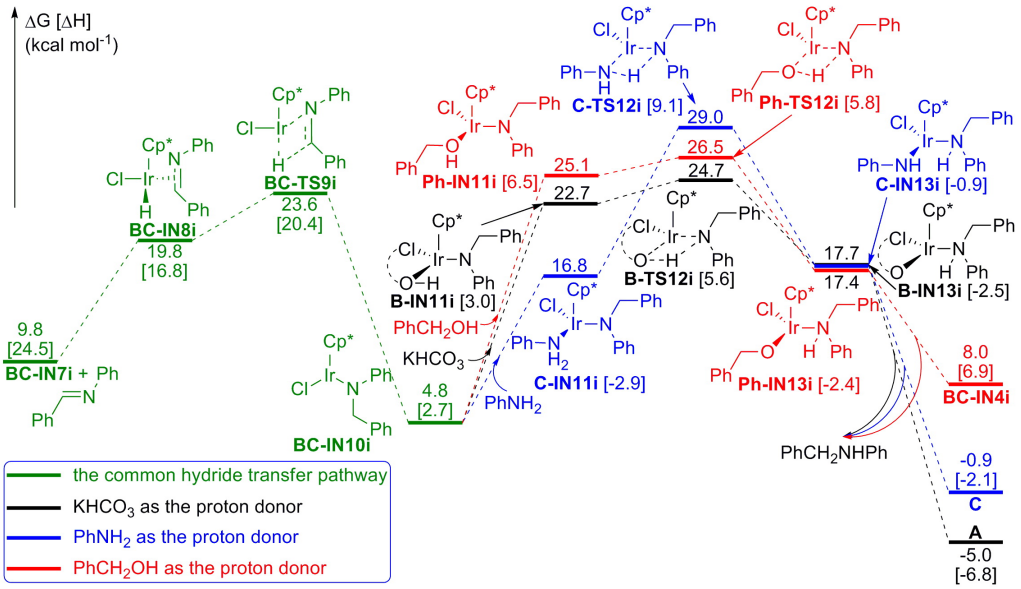

Fig. 10 Free energy profiles for the inner-sphere imine reduction with $KHCO_3$, $PhNH_2$, and $PhCH_2OH$ as the proton donors, respectively.

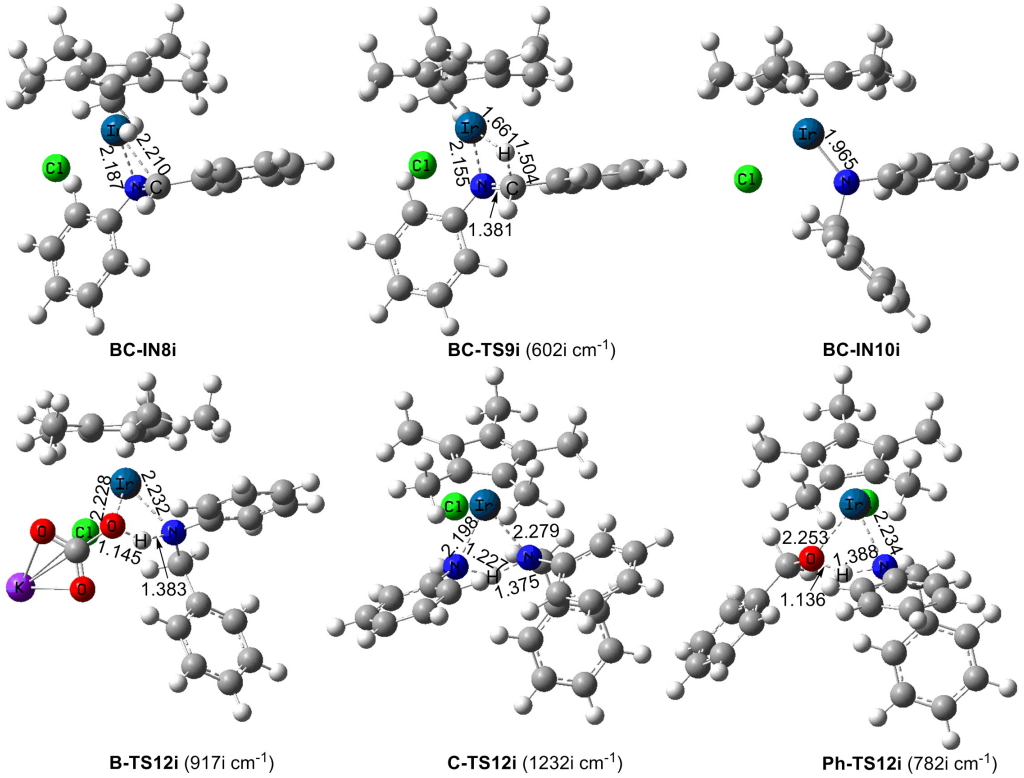

Fig. 11 Optimized structures of the key stationary points with selected bond distances (in Å) shown in Fig. 10.

tained from this pathway is chosen as the initial species of all the possible imine reduction pathways. Next, we seek the most favorable imine reduction pathway by considering different beginning coordination geometries of all the possible

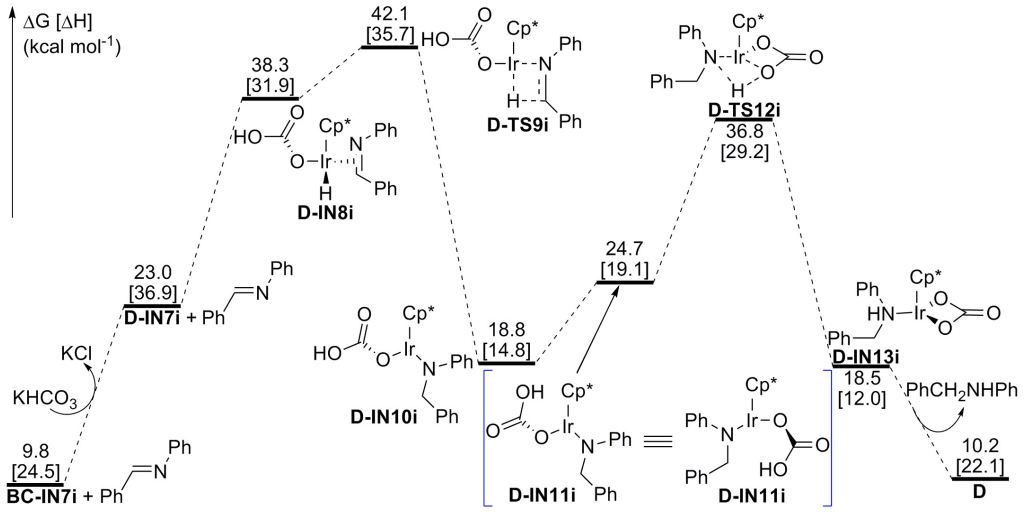

Fig. 12 Free energy profile for the inner-sphere imine reduction with **D-IN7i** as the reducing species.

hydrogen donors, inner-sphere and outer-sphere.

3.4.1 Inner-sphere imine reduction. The first scenario considered is the inner-sphere imine reduction pathways with $KHCO_3$, $PhNH_2$, and $PhCH_2OH$ as the proton donors, respectively. As shown in Fig. 10, coordination of the imine PhCH=NPh to the 16*e* Ir hydride **BC-IN7i** gives the starting intermediate **BC-IN8i**, in which the distances of Ir···N and Ir···C are 2.187 and 2.210 Å, respectively (see Fig. 11), indicating that the imine is η^2-bonded. This coordination process is favorable by 7.7 kcal mol^{-1} in enthalpy, but unfavorable by 10.0 kcal mol^{-1} in free energy owing to entropic penalty. The transition state **BC-TS9i** for the hydride transfer, only 3.8 kcal mol^{-1} higher than **BC-IN8i**, has a four-membered structure, in which the distances of Ir···H and C···H are 1.661 and 1.504 Å, respectively, confirming the Ir−H bond-breaking and C−H bond-forming processes. This hydride transfer affords Ir-amino intermediate **BC-IN10i**, which is only located at a free energy of 4.8 kcal mol^{-1} above the energy reference point.

Protonating the amino nitrogen of **BC-IN10i** to afford the final secondary amine product has three optional pathways, in which $KHCO_3$, $PhNH_2$, and $PhCH_2OH$ serve as the proton donors, respectively. As for $KHCO_3$ serving as the proton donor, the binding of $KHCO_3$ to **BC-IN10i** generates the intermediate **B-IN11i** and initiates the proton transfer process by costing a free energy of 17.9 kcal mol^{-1}. The transition state **B-TS12i** for the proton transfer is only 2.0 kcal mol^{-1} higher than **B-IN11i**, in which the proton is located between the Ir-bound oxygen and the amino nitrogen (O···H = 1.145 Å and N···H = 1.383 Å). This transition state connects to the secondary amine product $PhCH_2NHPh$-coordinated intermediate **B-IN13i**, which is 17.7 kcal mol^{-1} less stable than the energy reference point. However, a favorable free energy can promote the dissociation of $PhCH_2NHPh$ from **B-IN13i**. This dissociation results in the regeneration of complex **A** (or **B** which can easily isomerize to **A**, not shown in the free energy profile) and lowers the free energy of the system down by 22.7 kcal mol^{-1}.

As for $PhNH_2$ serving as the proton donor, the proton transfer process is similar to that with $KHCO_3$ as the proton donor. $PhNH_2$ first coordinates to **BC-IN10i** to give the intermediate **C-IN11i** by requiring a free energy of 12.0 kcal mol^{-1}. Then the proton transfers to the N atom of the $PhCH_2NPh$ moiety from the $PhNH_2$ ligand via the transition state **C-TS12i** with a relative free energy of 12.2 kcal mol^{-1} to **C-IN11i**, producing the secondary amine product $PhCH_2NHPh$-coordinated intermediate **C-IN13i**. **C-IN13i** could further dissociate into $PhCH_2NHPh$ and **C**.

As for $PhCH_2OH$ serving as the proton donor, the proton transfer process is similar to that with $KHCO_3$ or $PhNH_2$ as the proton donor. The starting $PhCH_2OH$-coordinated intermediate **Ph-IN11i** is 20.3 kcal mol^{-1} higher than **BC-IN10i** + $PhCH_2OH$. After passing through the transition state **Ph-TS12i** with a relative free energy of 1.4 kcal mol^{-1} to **Ph-IN11i**, the secondary amine product $PhCH_2NHPh$-coordinated intermediate **Ph-IN13i** is obtained, from which the release of the weakly bound secondary amine product is exergonic by 9.4 kcal mol^{-1}, and regenerates the alkoxide complex **BC-IN4i**.

The second scenario considered is the inner-sphere imine reduction pathway with **D-IN7i** (produced by the reaction of **BC-IN7i** with $KHCO_3$) as the reducing species, which is the same as Eisenstein and co-workers' proposed pathway.[21] As shown in Fig. 12, imine PhCH=NPh first coordinates to **D-**

IN7i to yield the intermediate **D-IN8i** by costing a free energy of 15.3 kcal mol^{-1}. After climbing the transition state **D-TS9i** with a relative free energy of 3.8 kcal mol^{-1} to **D-IN8i**, the amino intermediate **D-IN10i** is formed. However, **D-IN10i** can not directly undergo an intramolecular proton transfer reaction to give the secondary amine product $PhCH_2NHPh$. It must isomerize the complex **D-IN11i**, which could generate $PhCH_2NHPh$ and **D** via the transition state **D-TS12i**. Relative to **D-IN10i**, the free energies of **D-IN11i** and **D-TS12i** are 5.9 and 18.0 kcal mol^{-1}, respectively.

3.4.2 Outer-sphere imine reduction. The 16*e* complex **BC-IN7i** has a vacant site on the Ir center, so $KHCO_3$, $PhNH_2$, and $PhCH_2OH$ can coordinate to **BC-IN7i**, respectively, and generate the 18*e* complexes **B-IN3o**, **C-IN3o**, and **Ph-IN1o**. $KHCO_3$ could also react with **BC-IN7i** to afford another 18*e* complex **D-IN2o**. In the following, the outer-sphere imine reduction pathways with these complexes as the hydrogen donors will be considered, respectively.

In the case of **B-IN3o** serving as the reducing species, the imine PhCH=NPh binds with **B-IN3o** to form the beginning hydrogen-bonded intermediate **B-IN4o** by costing a free energy of 7.3 kcal mol^{-1} (Fig. 13). The transition state **B-TS5o**

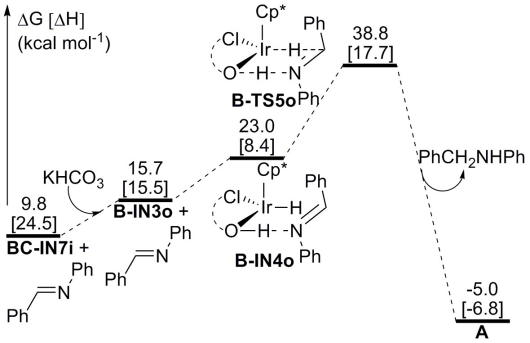

Fig. 13 Free energy profile for the outer-sphere imine reduction with **B-IN3o** as the reducing species.

for the concerted proton and hydride transfer, located at 15.8 kcal mol^{-1} above **B-IN4o**, has a six-membered structure, in which the distances of O···H, N···H, Ir···H, and C···H are 1.018, 1.712, 1.851, and 1.293 Å, respectively (Fig. 14). This transition state leads to the formation of the secondary amine product $PhCH_2NHPh$ and the regeneration of the complex **A**.

In the case of **C-IN3o** serving as the reducing species, the imine reduction with **C-IN3o** proceeds by way of the hydrogen-bonded intermediate **C-IN4o** (Fig. 15). Intermediate **C-IN4o** is 10.3 kcal mol^{-1} higher than **C-IN3o** + PhCH=NPh. The transition state **C-TS5o** for the concerted proton and hydride transfer with a relative free energy of 15.6 kcal mol^{-1} to **C-IN4o** also has a six-membered structure, in which the proton is located between the two nitrogens, and

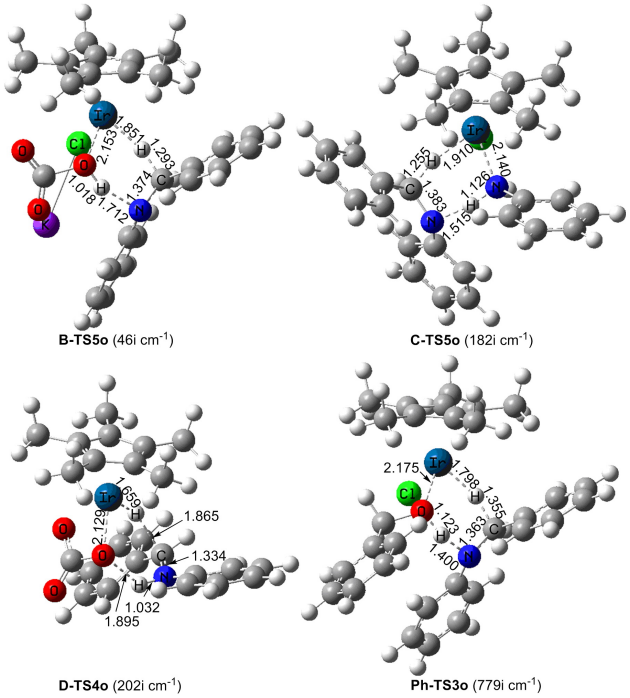

Fig. 14 Optimized structures of the key stationary points with selected bond distances (in Å) for the outer-sphere imine reduction.

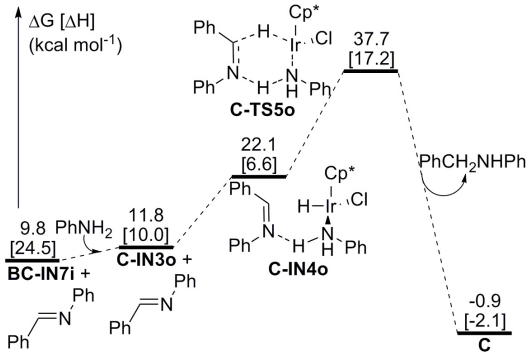

Fig. 15 Free energy profile for the outer-sphere imine reduction with **C-IN3o** as the reducing species.

the hydride lies midway between Ir and C (Fig. 14). This transition state results in the formation of the secondary amine product $PhCH_2NHPh$ and the regeneration of the complex **C**.

In the case of **Ph-IN1o** serving as the reducing species, the binding of PhCH=NPh to **Ph-IN1o** generates the initial intermediate **Ph-IN2o** by requiring a free energy of 6.3 kcal mol^{-1} (Fig. 16). After passing through the six-membered transition state **Ph-TS3o** with a relative free energy of 15.9 kcal mol^{-1} to **Ph-IN2o**, the secondary amine product $PhCH_2NHPh$ and the alkoxide complex **BC-IN4i** are obtained.

In the case of **D-IN2o** serving as the reducing species,

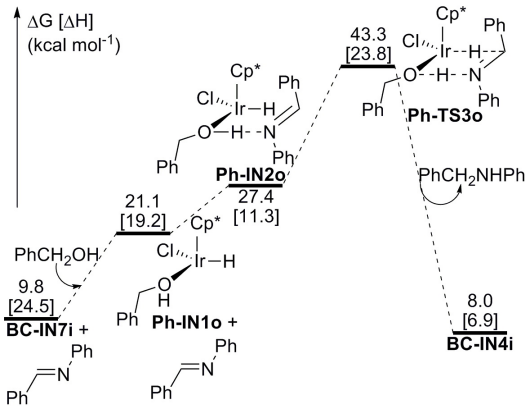

Fig. 16 Free energy profile for the outer-sphere imine reduction with **Ph-IN1o** as the reducing species.

the imine reduction takes place concertedly by passing through the hydrogen-bonded intermediate **D-IN3o** and the six-membered transition state **D-TS4o** (Fig. 17). Relative to

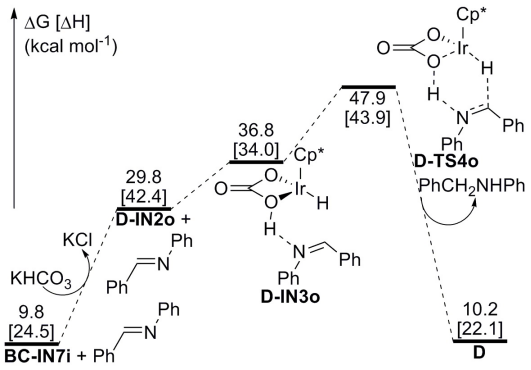

Fig. 17 Free energy profile for the outer-sphere imine reduction with **D-IN2o** as the reducing species.

D-IN2o + PhCH=NPh, the free energies of **D-IN3o** and **D-TS4o** are 7.0 and 18.1 kcal mol^{-1}, respectively. **D-TS4o** leads to the formation of the secondary amine product $PhCH_2NHPh$ and the regeneration of the complex **D**.

3.4.3 Comparison of different imine reduction pathways. In the above discussions of imine reduction, we proposed eight possible pathways: (1I) (Note: I denotes imine reduction) the inner-sphere imine reduction pathway with $KHCO_3$ as the proton donor (Fig. 10, green pathway + black pathway), (2I) the inner-sphere imine reduction pathway with $PhNH_2$ as the proton donor (Fig. 10, green pathway + blue pathway), (3I) the inner-sphere imine reduction pathway with $PhCH_2OH$ as the proton donor (Fig. 10, green pathway + red pathway), (4I) the inner-sphere imine reduction pathway with **D-IN7i** as the reducing species (Fig. 12), (5I) the outer-sphere imine reduction pathway with **B-IN3o** as the reducing species (Fig. 13), (6I) the outer-sphere imine reduction pathway with **C-IN3o** as the reducing species (Fig. 15), (7I) the outer-sphere imine reduction pathway with **Ph-IN1o** as the reducing species (Fig. 16), and (8I) the outer-sphere imine reduction pathway with **D-IN2o** as the reducing species (Fig. 17). For pathways 1I-8I, the activation free energy barriers are 19.9, 24.2, 21.7, 32.3, 29.0, 27.9, 33.5, and 38.1 kcal mol^{-1}, respectively, and the reaction free energies are -14.8, -10.7, -1.8, +0.4, -14.8, -10.7, -1.8, and +0.4, kcal mol^{-1}, respectively. On the basis of these calculation results, we can draw the following conclusions: (1) Pathway 1I is the most favorable imine reduction pathway both kinetically and thermodynamically. (2) Pathway 3I is the second favorable imine reduction pathway. (3) Other imine reduction pathways cannot compete with 1I, and thus can be ruled out safely.

3.5 Discussion with the energetic span model

The above discussions indicate that 2A-1I is the most favorable catalytic cycle. To further confirm this conclusion and look for rate-affecting key states, we calculated TOFs and degrees of TOF control (X_i) for the six lower-energy pathways using the Fortran program[43] based on the energetic span model.[44,45] The calculated results are shown in Table 1, from

Table 1 TOF values (in h^{-1}), key state energies (in kcal mol^{-1}) and degrees of TOF control for the six lower-energy pathways

pathway/TOF	TDI/X_I	TDTS/$\Delta G/X_T$	STDTS/$\Delta G/X_T$
1A-1I/1.84	**A**/1.00	**B-TS2i**/28.1/0.68	**BC-TS5i**/27.5/0.31
1A-2I/0.58	**A**/0.99	**C-TS12i**/29.0/0.69	**B-TS2i**/28.1/0.21
1A-3I/1.69	**A**/1.00	**B-TS2i**/28.1/0.63	**BC-TS5i**/27.5/0.29
2A-1I/4.68	**A**/1.00	**BC-TS5i**/27.5/0.82	**C-TS2i**/25.9/0.10
2A-2I/0.68	**A**/0.99	**C-TS12i**/29.0/0.86	**BC-TS5i**/27.5/0.12
2A-3I/3.96	**A**/0.99	**BC-TS5i**/27.5/0.68	**Ph-TS12i**/26.5/0.18

which we get the following results: (1) 2A-1I has the highest TOF, 4.68 h^{-1}, confirming that 2A-1I is the most favorable catalytic cycle. (2) The TDI and the TDTS are the 18*e* complex **A** with $X_I = 1.00$ and the transition state **BC-TS5i** for β-H elimination with $X_T = 0.82$, respectively. (3) The energetic span is 27.5 kcal mol^{-1}. (4) 2A-3I becomes the second favorable catalytic cycle since it has the second highest TOF, 3.96 h^{-1}. 2A-3I and 2A-1I have the identical TDI and TDTS. It is the secondary TDTS (STDTS) **Ph-TS12i** in 2A-3I, slightly higher than the STDTS **C-TS2i** in 2A-1I, that makes 2A-3I the second favorable catalytic cycle. (5) 1A-1I and 1A-3I are the third and the fourth favorable catalytic cycles, respectively. They have the identical TDI, TDTS, and STDTS. The TOF difference between 1A-1I and 1A-3I is caused by the proton transfer transition states for imine reduction, **B-TS12i** in 1A-1I and **Ph-TS12i** in 1A-3I (not shown in Table 1). (6) Other

catalytic cycles are unfavorable. On the basis of results 4 and 5, we can also know that neither a transition state nor a reaction step could determine the TOF of a catalytic cycle.[45]

To test the functional and basis sets dependence, we selected some complexes, which were necessary for the TOF calculations, from catalytic cycles 2A-1I, 2A-3I, and 1A-1I, and recalculated their energies. The key state energies and TOF values are shown in Table 2 (see the Supplementary Information for other energies). All the calculated TOFs consistently support that 2A-1I is the most favorable catalytic cycle.

Table 2 Key state energies (in kcal mol^{-1}) at different DFT levels and TOF values (in h^{-1})

key state	M06//B3LYP[a]	M06//B3PW91	M06//PBE1PBE	M06//M06
BC-TS5i	27.5(27.3)	28.3	28.3	27.9
C-TS2i	25.9(24.5)	25.4	24.4	25.3
TOF in 2A-1I	4.68(6.84)	1.91	1.91	2.23
Ph-TS12i	26.5(25.5)	26.5	26.5	31.7
TOF in 2A-3I	3.96(6.48)	1.80	1.84	0.0234
B-TS2i	28.1(27.5)	27.5	26.3	30.6
TOF in 1A-1I	1.84(3.31)	1.51	1.80	0.0972

[a] Values in parentheses were obtained at the M06/BSIV//B3LYP/BSIII level (BSIII: the basis set combination of SDDALL with an extra f polarization basis function (exponent 0.938) for Ir and 6-31G(d,p) for all the other atoms; BSIV: the basis set combination of SDDALL with an extra f polarization basis function (exponent 0.938) for Ir and 6-311++G(2df,2p) for all the other atoms).

4 Conclusions

We have carried out a thorough theoretical study on the reaction mechanism of $[Cp^*IrCl_2]_2/K_2CO_3$-catalyzed N-alkylation of amines with alcohols using DFT calculations. The calculation results reveal that this N-alkylation reaction proceeds via the hydrogen autotransfer mechanism and the catalytic cycle includes three sequential stages: (1) alcohol oxidation, (2) imine formation, (3) imine reduction. For alcohol oxidation, the inner-sphere hydrogen transfer pathway under the catalysis of $Cp^*Ir(NHPh)Cl$ (i.e. pathway 2A) is the most favorable. This pathway consists of three successive steps: (I) The precatalyst $[Cp^*IrCl_2]_2$ is activated by K_2CO_3 and $PhNH_2$ to generate the active catalyst $Cp^*Ir(NHPh)Cl$ (Fig. 1); (II) The hydroxyl hydrogen of benzyl alcohol transfers to the $PhNH^-$ ligand in the form of the proton to give the alkoxide complex **BC-IN4i** (Fig. 3, blue pathway); (III) The β-H atom transfers to the Ir atom to afford benzaldehyde and the Ir hydride **BC-IN7i** (Fig. 3, green pathway). The activation free energy barrier for the β-H elimination is as high as 27.5 kcal mol^{-1}, which accounts for the high temperature required to obtain an acceptable rate. For imine reduction, the inner-sphere hydrogen transfer pathway with $KHCO_3$ as the proton donor (i.e. pathway 1I) is the most favorable. This pathway consists of two successive steps: (I) The hydride transfers to the C atom of the C=N bond from the Ir atom of **BC-IN7i** to give the amino complex **BC-IN10i** (Fig. 10, green pathway); (II) The proton transfers to the N atom from the $KHCO_3$ ligand to produce the secondary amine product and regenerate the complex **A** (Fig. 10, black pathway). Alcohol oxidation and imine formation are thermodynamically endergonic by 6.9 and 2.9 kcal mol^{-1}, respectively, but imine reduction is thermodynamically exergonic by 14.8 kcal mol^{-1}. Therefore, imine reduction is the driving force for the catalytic cycle.

We also use the energetic span model to assess the most favorable catalytic cycle 2A-1I. Degrees of TOF control show that the TDI and the TDTS are the 18*e* complex **A** ($X_I = 1.00$) and the transition state **BC-TS5i** for β-H elimination ($X_T = 0.82$), respectively. The calculated TOF, 4.68 h^{-1}, is in agreement with experimental yield (Benzylaniline was obtained in a GC yield of 100% under the experimental conditions (see eq 1)), which provides strong support for the proposed catalytic cycle. This theoretical study will provide useful information for further research and utilization of the transition metal-catalyzed N-alkylation reaction of amines with alcohols.

Acknowledgements

The authors thank the National Basic Research Program of China (973 Program; 2012CB932800), the National Natural Science Foundation of China (No.21303067, No.21373099, No.11447194), and Doctoral Fund of Ministry of Education of China (No.20130061110020) for financial support of this research. The authors also thank Mathematics Experiment Center, Jilin Institute of Chemical Technology, for computer support.

References

1 (a) C. L. Allen and J. M. Williams, *Chem. Soc. Rev.*, 2011, **40**, 3405-3415; (b) G. R. Maxwell, *Synthetic Nitrogen Products: A Practical Guide to the Products and Processes*, Kluwer Academic Publishers, New York, 2004; (c) S. A. Lawrence, *Amines: Synthesis, Properties and Applications*, Cambridge University Press, Cambridge, 2004.

2 (a) O. Navarro, N. Marion, J. Mei and S. P. Nolan, *Chem.-Eur. J.*, 2006, **12**, 5142-5148; (b) J. F. Hartwig, *Synlett*, 2006, **9**, 1283-1294; (c) X. Li, E. A. Mintz, X. R. Bu, O. Zehnder, C. Bosshard and P. Gunter, *Tetrahedron*, 2000, **56**, 5785-5791; (d) J. P. Wolfe and S. L. Buchwald, *J. Am. Chem. Soc.*, 1997, **119**, 6054-6058.

3 (a) T. Mizuta, S. Sakagushi and Y. Ishii, *J. Org. Chem.*, 2005, **70**, 2195-2199; (b) A. F. Abdel-Magid, K. G. Car-

son, B. D. Harris, C. A. Maryan-off and R. D. Shah, *J. Org. Chem.*, 1996, **61**, 3849-3862; (c) S. Bhattacharyya, *J. Org. Chem.*, 1995, **60**, 4928-4929.

4 (a) S. Werkmeister, S. Fleischer, S. L. Zhou, K. Junge and M. Beller, *ChemSusChem*, 2012, **5**, 777-782; (b) S. Pan, K. Endo and T. Shibata, *Org. Lett.*, 2012, **14**, 780-783; (c) K. D. Hesp, S. Tobisch and M. Stradiotto, *J. Am. Chem. Soc.*, 2010, **132**, 413-426; (d) N. R. Perl, N. D. Ide, S. Prajapati, H. H. Perfect, S. G. Duron and D. Y. Gin, *J. Am. Chem. Soc.*, 2010, **132**, 1802-1803; (e) X. Shen and S. L. Buchwald, *Angew. Chem. Int. Ed.*, 2010, **49**, 564-567.

5 (a) M. Ahmed, A. M. Seayad, R. Jackstell and M. Beller, *J. Am. Chem. Soc.*, 2003, **125**, 10311-10318; (b) T. O. Vieira and H. Alper, *Chem. Commun.*, 2007, 2710-2711; (c) M. Ahmed, R. P. J. Bronger, R. Jackstell, P. C. J. Kamer, P. W. N. M. van Leeuwen and M. Beller, *Chem.-Eur. J.*, 2006, **12**, 8979-8988.

6 (a) S. Bähn, S. Imm, L. Neubert, M. Zhang, H. Neumann and M. Beller, *ChemCatChem*, 2011, **3**, 1853-1864; (b) G. Guillena, D. J. Ramón and M. Yus, *Chem. Rev.*, 2010, **110**, 1611-1641; (c) G. E. Dobereiner and R. H. Grabtree, *Chem. Rev.*, 2010, **110**, 681-703; (d) G. Guillena, D. J. Ramón and M. Yus, *Angew. Chem. Int. Ed.*, 2007, **46**, 2358-2364; (e) M. G. Edwards, R. F. Jazzar, B. M. Paine, D. J. Shermer, M. K. Whittlesey, J. M. J. Williams and D. D. Edney, *Chem. Commun.*, 2004, 90-91; (f) T. D. Nixon, M. K. Whittlesey and J. M. J. Williams, *Dalton Trans.*, 2009, **5**, 753-762.

7 R. Grigg, T. R. B. Mitchell, S. Sutthivaiyakit and N. Tongpenyai, *J. Chem. Soc., Chem. Commun.*, 1981, 611-612.

8 Y. Watanabe, Y. Tsuji and Y. Ohsugi, *Tetrahedron Lett.*, 1981, **22**, 2667-2670.

9 (a) T. T. Dang, B. Ramalingam, S. P. Shan and A. M. Seayad, *ACS Catal.*, 2013, **3**, 2536-2540; (b) A. Martínez-Asencio, M. Yus and D. J. Ramon, *Synthesis*, 2011, 3730-3740.

10 (a) Y. Liu, W. Chen, C. Feng and G. Deng, *Chem.-Asian J.*, 2011, **6**, 1142-1146; (b) S. Imm, S. Bähn, L. Neubert, H. Neumann and M. Beller, *Angew. Chem. Int. Ed.*, 2010, **49**, 8126-8129; (c) A. B. Enyong and B. Moasser, *J. Org. Chem.*, 2014, **79**, 7553-7563; (d) M. H. S. A. Hamid, C. L. Allen, G. W. Lamb, A. C. Maxwell, H. C. Maytum, A. J. A. Watson and J. M. J. Williams, *J. Am. Chem. Soc.*, 2009, **131**, 1766-1774; (e) N. J. Oldenhuis, V. M. Dong and Z. Guan, *J. Am. Chem. Soc.*, 2014, **136**, 12548-12551.

11 S. L. Feng, C. Z. Liu, Q. Li, X. C. Yu and Q. Xu, *Chin. Chem. Lett.*, 2011, **22**, 1021-1024.

12 (a) O. Saidi and J. M. J. Williams, *Iridium catalysis, Top. Organomet. Chem.*, 2011, **34**, 77-106; (b) A. Prades, R. Corberan, M. Poyatos and E. Peris, *Chem.-Eur. J.*, 2008, **14**, 11474-11479; (c) Y. H. Chang, Y. Nakajima and F. Ozawa, *Organometallics*, 2013, **32**, 2210-2215.

13 K.-i. Fujita, Z. Li, N. Ozeki and R. Yamaguchi, *Tetrahedron Lett.*, 2003, **44**, 2687-2690.

14 (a) O. Saidi, A. J. Blacker, G. W. Lamb, S. P. Marsden, J. E. Taylor and J. M. Williams, *Org. Process Res. Dev.*, 2010, **14**, 1046-1049; (b) K.-i. Fujita, T. Fujii and R. Yamaguchi, *Org. Lett.*, 2004, **6**, 3525-3528; (c) K.-i. Fujita, Y. Enoki and R. Yamaguchi, *Tetrahedron*, 2008, **64**, 1943-1954.

15 M. Zhu, K.-i. Fujita and R. Yamaguchi, *Org. Lett.*, 2010, **12**, 1336-1339.

16 R. Yamaguchi, S. Kawagoe, C. Asai and K.-i. Fujita, *Org. Lett.*, 2008, **10**, 181-184.

17 (a) A. Wetzel, S. Wöckel, M. Schelwies, M. K. Brinks, F. Rominger, P. Hofmann and M. Limbach, *Org. Lett.*, 2013, **15**, 266-269; (b) R. Kawahara, K.-i. Fujita and R. Yamaguchi, *Adv. Synth. Catal.*, 2011, **353**, 1161-1168; (c) J. Q. Li and P. G. Andersson, *Chem. Commun.*, 2013, **49**, 6131-6133; (d) A. Bartoszewicz, R. Marcos, S. Sahoo, A. K. Inge, X. Zou and B. Martín-Matute, *Chem.-Eur. J.*, 2012, **18**, 14510-14519.

18 (a) A. Martínez-Asencio, D. J. Ramon and M. Yus, *Tetrahedron Lett.*, 2010, **51**, 325-327; (b) X. J. Cui, F. Shi, M. K. Tse, D. Gordes, K. Thurow, M. Beller and Y. Q. Deng, *Adv. Synth. Catal.*, 2009, **351**, 2949-2958; (c) A. Martínez-Asencio, D. J. Ramon and M. Yus, *Tetrahedron*, 2011, **67**, 3140-3149.

19 (a) Y. S. Zhao, S. W. Foo and S. Saito, *Angew. Chem. Int. Ed.*, 2011, **50**, 3006-3009; (b) X. J. Cui, F. Shi, Y. Zhang and Y. Q. Deng, *Tetrahedron Lett.*, 2010, **51**, 2048-2051; (c) P. KumaráVerma, *Green Chem.*, 2013, **15**, 1687-1693.

20 K.-i. Fujita, K. Yamamoto and R. Yamaguchi, *Org. Lett.*, 2002, **4**, 2691-2964.

21 D. Balcells, A. Nova, E. Clot, D. Gnanamgari, R. H. Crabtree and O. Eisenstein, *Organometallics*, 2008, **27**, 2529-2535.

22 P. Fristrup, M. Tursky and R. Madsen, *Org. Biomol. Chem.*, 2012, **10**, 2569-2577.

23 (a) H. Li, G. Lu, J. Jiang, F. Huang and Z.-X. Wang, *Organometallics*, 2011, **30**, 2349-2363; (b) J.-W. Handgraaf, J. N. H. Reek and E. J. Meijer, *Organometallics*, 2003, **22**, 3150-3157; (c) K. H. Hopmann and A. Bayer, *Organometallics*, 2011, **30**, 2483-2497.

24 G. M. Zhao, H. L. Liu, D. D. Zhang, X. R. Huang and X. Yang, *ACS Catal.*, 2014, **4**, 2231-2240.

25 (a) M. Yamakawa, H. Ito and R. Noyori, *J. Am. Chem. Soc.*, 2000, **122**, 1466-1478; (b) J.-W. Handgraaf and E. J. Meijer, *J. Am. Chem. Soc.*, 2007, **129**, 3099-3103; (c) A. Nova, D. Balcells, N. D. Schley, G. E. Dobereiner, R. H. Crabtree and O. Eisenstein, *Organometallics*, 2010, **29**, 6548-6558; (d) J. Bosson, A. Poater, L. Cavallo and S. P.

Nolan, *J. Am. Chem. Soc.*, 2010, **132**, 13146-13149; (e) A. Comas-Vives, G. Ujaque and A. Lledós, *Organometallics*, 2007, **26**, 4135-4144; (f) T. Privalov, J. S. M. Samec and J.-E. Bäckvall, *Organometallics*, 2007, **26**, 2840-2848.

26 M. J. Frisch, G. W. Trucks, H. B. Schlegel, G. E. Scuseria, M. A. Robb, J. R. Cheeseman, G. Scalmani, V. Barone, B. Mennucci, G. A. Petersson, H. Nakatsuji, M. Caricato, X. Li, H. P. Hratchian, A. F. Izmaylov, J. Bloino, G. Zheng, J. L. Sonnenberg, M. Hada, M. Ehara, K. Toyota, R. Fukuda, J. Hasegawa, M. Ishida, T. Nakajima, Y. Honda, O. Kitao, H. Nakai, T. Vreven, J. A. Montgomery, Jr., J. E. Peralta, F. Ogliaro, M. Bearpark, J. J. Heyd, E. Brothers, K. N. Kudin, V. N. Staroverov, R. Kobayashi, J. Normand, K. Raghavachari, A. Rendell, J. C. Burant, S. S. Iyengar, J. Tomasi, M. Cossi, N. Rega, J. M. Millam, M. Klene, J. E. Knox, J. B. Cross, V. Bakken, C. Adamo, J. Jaramillo, R. Gomperts, R. E. Stratmann, O. Yazyev, A. J. Austin, R. Cammi, C. Pomelli, J. W. Ochterski, R. L. Martin, K. Morokuma, V. G. Zakrzewski, G. A. Voth, P. Salvador, J. J. Dannenberg, S. Dapprich, A. D. Daniels, O. Farkas, J. B. Foresman, J. V. Ortiz, J. Cioslowski and D. J. Fox, *Gaussian 09, Revision A.01*, Gaussian, Inc., Wallingford CT, 2009.

27 A. D. Becke, *J. Chem. Phys.*, 1993, **98**, 5648-5652.

28 C. Lee, W. Yang and R. G. Parr, *Phys. ReV. B*, 1988, **37**, 785-789.

29 A. V. Marenich, C. J. Cramer and D. G. Truhlar, *J. Phys. Chem. B*, 2009, **113**, 6378-6396.

30 D. Andrae, U. Häußermann, M. Dolg, H. Stoll and H. Preuß, *Theor. Chim. Acta.*, 1990, **77**, 123-141.

31 W. J. Hehre, R. Ditchfield and J. A. Pople, *J. Chem. Phys.*, 1972, **56**, 2257-2261.

32 (a) K. Fukui, *J. Phys. Chem.*, 1970, **74**, 4161-4163; (b) K. Fukui, *Acc. Chem. Res.*, 1981, **14**, 363-368.

33 (a) Y. Zhao and D. G. Truhlar, *J. Chem. Phys.*, 2006, **125**, 194101-194118; (b) Y. Zhao and D. G. Truhlar, *Acc. Chem. Res.*, 2008, **41**, 157-167.

34 F. Weigend and R. Ahlrichs, *Phys. Chem. Chem. Phys.*, 2005, **7**, 3297-3305.

35 A. Bergner, M. Dolg, W. Küchle, H. Stoll and H. Preuss, *Mol. Phys.*, 1993, **80**, 1431-1441.

36 J. P. Perdew and Y. Wang, *Phys. ReV. B*, 1992, **45**, 13244-13249.

37 M. Ernzerhof and G. E. Scuseria, *J. Chem. Phys.*, 1999, **110**, 5029-5036.

38 C. Song, S. Qu, Y. Tao, Y. Dang and Z.-X. Wang, *ACS Catal.*, 2014, **4**, 2854-2865.

39 R. Kawahara, K.-i. Fujita and R. Yamaguchi, *J. Am. Chem. Soc.*, 2010, **132**, 15108-15111.

40 N. E. Hall and B. J. Smith, *J. Phys. Chem. A*, 1998, **102**, 4930-4938.

41 H. Li, X. Wang, M. Wen and Z.-X. Wang, *Eur. J. Inorg. Chem.*, 2012, **31**, 5011-5020.

42 H. Li, X. Wang, F. Huang, G. Lu, J. Jiang and Z.-X. Wang, *Organometallics*, 2011, **30**, 5233-5247.

43 M. À. Carvajal, S. Kozuch and S. Shaik, *Organometallics*, 2009, **28**, 3656-3665.

44 (a) C. Amatore and A. Jutand, *J. Organomet. Chem.*, 1999, **576**, 254-278; (b) S. Kozuch and S. Shaik, *J. Am. Chem. Soc.*, 2006, **128**, 3355-3365; (c) S. Kozuch and S. Shaik, *J. Phys. Chem. A*, 2008, **112**, 6032-6041.

45 S. Kozuch and S. Shaik, *Acc. Chem. Res.*, 2011, **44**, 101-110.